Spatial Intensity Nonuniformities of an OMEGA Beam due to Nonlinear Beam Propagation

Several applications require that a laser beam maintain a high degree of wavefront quality after propagating a long distance through air. In particular, laser drivers for inertial confinement fusion use intense laser beams that propagate tens of meters through air to a fusion target. Many amplification stages are required in the system to reach the energy levels required for each beam. Good beam quality is essential throughout the system to prevent the onset of nonlinear effects that can lead to optical damage or wavefront degradation. To maintain beam quality, spatial filters are used between amplification stages to remove high-spatial-frequency modulation impressed onto the beams by random or fixed phase distortions in the beam paths. Despite the use of spatial filters, the wavefront quality of a high-energy laser can be degraded, and nonlinear optical effects can occur in the system.

Forward stimulated rotational Raman scattering (SRRS) can be generated when intense laser fields propagate through air[1–3] due to the N_2 molecules in the interaction path. This unwanted Raman radiation can degrade the spatial as well as the temporal characteristics of the beam. In addition, when a high-energy laser is focused into a spatial filter, the residual material remaining in the spatial filter can act as a nonlinear medium to again degrade the beam quality.

It is well known that for Raman scattering the coupling between the Raman Stokes and anti-Stokes radiation in a dispersive medium leads to the generation of conical emission.[4] The Stokes and anti-Stokes radiation is emitted at angles to the optical axis due to phase matching and is azimuthally symmetric about the optical axis. If the cylindrical symmetry of the pump wave is broken, then another phase-matched four-wave-mixing process can break the azimuthal symmetry of the conical emission, and a transverse modulational instability can occur. This instability manifests itself as preferential gain at six angles uniformly spaced around the cone, resulting in six intensity peaks around the cone resembling a hexagonal intensity distribution in the far field. Evidence of this four-wave-mixing convective instability was first reported by Tan-No *et al.*[5] in 1980. Since then several other observations have been reported along with several theoretical analyses.[5–13] The majority of the work in this field has been performed with counter-propagating pump beams in a nonlinear medium. A notable exception is the work of Pender and Hesselink,[9] who observed this instability with a single forward pump wave as in the experiments performed with the OMEGA laser to be discussed here.

Two separate experiments were performed with the OMEGA laser that show evidence of this transverse modulational instability. In the first experiment a beam underwent free propagation through air, and the instability was observed in the presence of SRRS. In the second experiment a 1-kJ laser was focused into a vacuum spatial filter having a 50-μm residual fill pressure, and the instability was observed in the near field after the spatial filter. These experiments illustrate that in order to determine the details of the spatial structure of an intense beam propagating in a nonlinear medium, this four-wave-mixing transverse modulational instability must be considered.

Experiments

Two separate experiments that exhibit transverse modulational instabilities were performed. In one experiment, the generation of SRRS in air was studied to determine the effects of SRRS on the propagation of OMEGA Upgrade beams as they propagate through air to a target. In another experiment the requirements on the final fill pressure for high-energy spatial filters was studied.

In the first experiment[2] a third-harmonic beam at 351-nm wavelength 600-ps full-width at half-maximum (FWHM) from the OMEGA laser was down collimated to approximately a 5-cm beam diameter and propagated over a 35-m path length in air. The near-field beam intensity profile was recorded on film at the beginning and end of the beam path. The spectral content of the beam was also recorded on film at the end of the air path using a 1-m spectrometer. The film was

developed, digitized with a microdensitometer, and converted to intensity exposure by using the appropriate film-density, log-intensity calibration for the film and for the experimental conditions used.

The spectrum, displayed in Fig. 59.11, clearly shows the generation of Stokes and anti-Stokes radiation from the SRRS process in air. For this experiment approximately 1% of the laser energy was converted to SRRS.

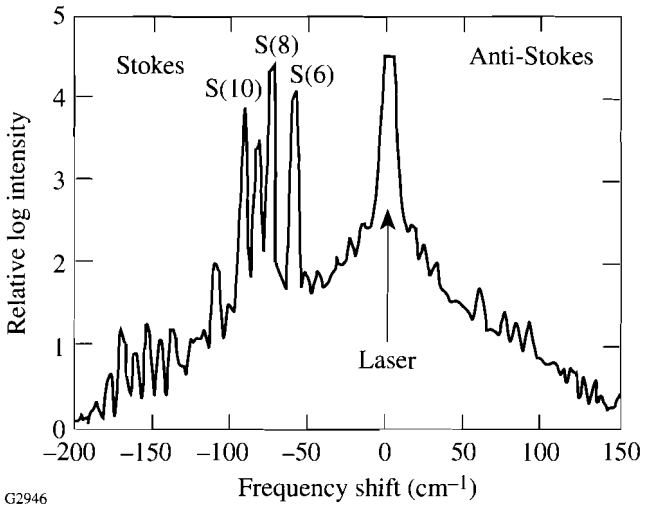

Figure 59.11
Raman spectrum showing several of the *S* transitions of nitrogen in air. The pump laser saturated the film at a frequency shift equal to zero.

The intensity distribution at the end of the 35-m air path is shown on a log scale in Fig. 59.12, where strong intensity modulation can be seen. To determine the spatial frequency content of the beam at the end of the air path, a two-dimensional FFT was calculated from the measured intensity distribution. To highlight the features in the FFT, the central portion of the FFT (containing the near dc spatial components) was blocked, and the FFT was plotted on a log scale, as shown in Fig. 59.13. Although the FFT is symmetric about positive and negative frequencies, it clearly shows evidence of the hexagonal pattern in the far field associated with the transverse modulational instability.

In the second experiment a beam with 1 kJ of energy, 700-ps FWHM, and a 1054-nm wavelength was focused into a spatial filter. The spatial filter input and output beam diameters were 18 cm, and the *f* number of the spatial filter was equal to 14. In an attempt to determine the maximum fill pressure allowed for this spatial filter with these beam param-

Figure 59.12
Near-field intensity distribution of the beam after propagating 35 m in air, plotted on a log scale.

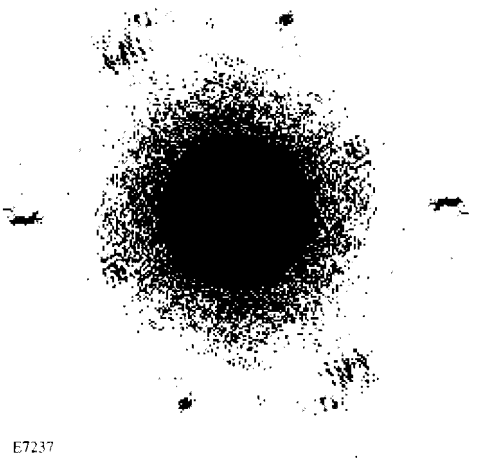

Figure 59.13
FFT of the near-field intensity distribution of the beam after propagating 35 m in air. The central portion of the FFT containing the low spatial frequencies was blocked, and the remaining FFT was plotted on a log scale. The hexagonal intensity distribution surrounding the central spot can be seen and is caused by the transverse modulational instability.

eters, the fill pressure was varied, and the beam intensity distribution after the spatial filter was recorded on film. The film was again digitized and intensity converted. The input beam to the spatial filter was slightly astigmatic. The intensity modulation on the beam exiting the spatial filter with a 50-μm residual fill pressure (the highest pressure used in the experiments) is shown in Fig. 59.14. To enhance the intensity modulational features on the image of the beam, a constant intensity (equal to 80% of the maximum intensity) was subtracted from the digitized near-field intensity distribution of the beam. The results are shown in Fig. 59.14. In this figure a hexagonal intensity distribution can be seen at the approximate center of the distribution centered on the cross with a diameter approximately equal to the beam radius. Additional modulation at the edges of the intensity distribution can also be seen. For this experiment, no measurements were made of the spectral content of the beam.

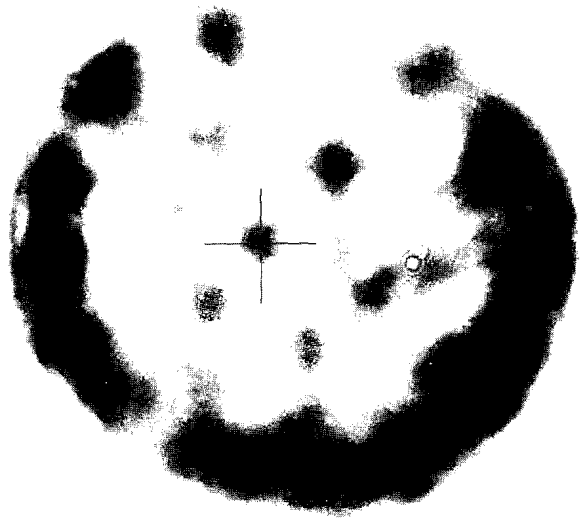

E7238

Figure 59.14
Near-field intensity distribution of a 1-kJ beam at 1054-nm wavelength after propagating through a spatial filter with a 50-μm residual fill pressure. To help illustrate the modulation, 80% of the beam intensity was subtracted from the image. The hexagonal intensity distribution caused by the transverse modulational instability can be seen centered on the cross with a diameter approximately equal to the beam radius.

The above experiments show evidence of a transverse modulational instability with a high-energy laser. The observed hexagonal intensity distributions are characteristic of a four-wave-mixing interaction that can be understood through simple modeling using the plane-wave approximation.

Theory and Discussion

Stokes and anti-Stokes SRRS will be generated when an intense laser beam propagates over a long path in air. Appreciable amounts of this radiation are created when the product of the laser intensity times the interaction length exceeds a minimum threshold. In a dispersive medium, the coupling between the Stokes and anti-Stokes fields leads to conical emission. If the pump laser is not cylindrically symmetric, then the coupling between the Stokes and anti-Stokes fields can lead to the observed transverse modulational instability.

To see the origin of this transverse modulational instability we follow the analysis of Pender and Hesselink[9] and begin with the wave equation in a Raman active medium:

$$\nabla^2 E - \frac{n^2}{c^2}\frac{\partial^2 E}{\partial t^2} = \frac{4\pi}{c^2}\frac{\partial^2 P^{NL}}{\partial t^2}, \tag{1}$$

where the nonlinear polarization is given by

$$P^{NL} = \chi^{(3)} E^3 . \tag{2}$$

We assume that the seven waves making up the hexagonal intensity distribution (the six waves uniformly spaced around the cone plus one on axis) are all linearly polarized, have the same frequency (such as all Stokes frequencies), and propagate in the near forward direction (i.e., no counterpropagating beams). For clarity the seven waves are shown in Fig. 59.15. In the plane wave approximation we assume that the total electric field E is given by the sum of the laser field and a sum over seven Stokes and seven anti-Stokes fields. With these assumptions, the total electric field in the medium is given by

$$E = E_L e^{-i(\omega_L t + \mathbf{k}_L \cdot \mathbf{z})} + \sum_{j=0}^{6} E_{Sj} e^{-i(\omega_S t + \mathbf{k}_{Sj} \cdot \mathbf{z})} + \sum_{j=0}^{6} E_{Aj} e^{-i(\omega_A t + \mathbf{k}_{Aj} \cdot \mathbf{z})} + cc, \tag{3}$$

where the subscripted E's are the amplitudes of waves with frequency ω and wave vector $\mathbf{k}$, and the subscripts L, S, and A denote the laser, Stokes, and anti-Stokes fields, respectively. If we cube this total electric field, substitute into the optical wave Eq. (1) with the appropriate nonlinear polarization [Eq. (2)], and make the standard assumptions in steady state, we get for a typical Stokes field ($S1$ in Fig. 59.15, for example)

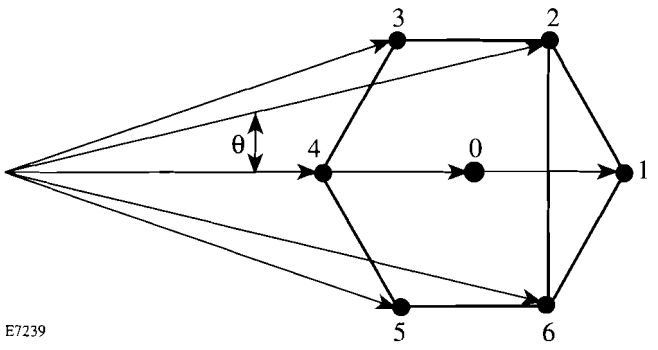

Figure 59.15
Diagram of the seven beams making up the hexagonal intensity distribution characteristic of the transverse modulational instability.

$$\frac{\partial E_{S1}}{\partial z} = -i\gamma\left\{|E_L|^2 + \sum_{j=0}^{6}|E_{Aj}|^2 + \sum_{j=0}^{6}|E_{Sj}|^2 - \frac{1}{2}|E_{S1}|^2\right\}E_{S1}$$

$$-i\frac{\gamma}{2}E_L^2E_{A4}^*\exp[-i\Delta k_{A4}z]$$

$$-i\frac{\gamma}{2}E_{S0}^*E_{S2}E_{S6}\exp[+i\Delta kz]$$

$$-i\frac{\gamma}{2}E_{S0}\left(E_{S2}E_{S3}^* + E_{S6}E_{S5}^*\right)\exp[-i\Delta kz]$$

$$-i\frac{\gamma}{2}E_{S4}^*E_{S0}^2\exp[-i2\Delta kz]$$

$$-i\frac{\gamma}{2}E_{S4}^*\left(E_{S2}E_{S5} + E_{S3}E_{S6}\right) \qquad (4)$$

with $\Delta k_{Aj} = \left(2\mathbf{k}_L - \mathbf{k}_{S1} - \mathbf{k}_{Aj}\right)\cdot\mathbf{z}$ and $\Delta k = k(1-\cos\theta)$ and where θ is the cone angle for Stokes and anti-Stokes coupling and γ is the coupling coefficient. This equation describes the evolution of one of the Stokes waves (wave $S1$) in the medium and has many contributions that will be discussed further to provide insight into the nature of the instability.

The first term on the right in Eq. (4) contains the intensity-induced refractive index terms and gives rise to ordinary stimulated scattering. The second term on the right is the Raman Stokes and anti-Stokes coupling term that can be completely phased matched $\left(\Delta k_{Aj} = 0\right)$, even in a dispersive medium. In a dispersive medium phase matching occurs when the Stokes and anti-Stokes fields propagate at some angle to the optical axis giving rise to conical emission. (This second term has azimuthal symmetry and is present for any choice of Stokes wave around the cone.)

The third and fourth terms are largely responsible for the transverse modulational instability. The third term on the right is a near-phase-matched, four-wave-mixing term and gives rise to loss for $S1$, i.e., one photon is absorbed from each of beams $S0$ and $S1$ and reemitted into beams $S2$ and $S6$. Near complete phase matching for this process occurs and can be seen from Fig. 59.15 since a line drawn through $S2$ and $S6$ and a line drawn through $S0$ and $S1$ bisect one another. (A small phase mismatch Δkz exists due to the off-axis propagation of the waves involved. Perfect phase matching would occur only for all waves propagating in the forward direction; however, the additional gain provided in this off-axis direction by ordinary conical emission outweighs the loss due to this phase mismatch.) In a similar manner, the fourth term on the right contains two near-phase-matched (by the same argument given for the third term), four-wave-mixing terms. These contributions give rise to additional gain for $S1$ at the expense of the pair of waves $S2$ and $S3$ and the pair $S5$ and $S6$. Hence, hexagonal position $S1$ has two gain contributions [Eq. (4), term (4)] and one loss contribution [Eq. (4), term (3)] resulting in net gain due to the four-wave-mixing process associated with the transverse modulational instability. This implies that if Stokes wave $S1$ is present, it will lead to the efficient generation of the other Stokes waves around the hexagon since we can rotate the cone by 60° and repeat the argument. The location of $S1$ along the cone, however, is arbitrary, and for an azimuthally symmetric pump laser we would expect ordinary conical emission. If, on the other hand, the pump laser is not perfectly symmetric about the optic axis, then the Stokes wave at $S1$ may experience higher gain than the other waves around the cone, which will initiate the instability leading to the formation of the hexagonal intensity distribution.

The fifth and sixth terms on the right are terms that contribute to uniform gain around the cone and, hence, do not contribute to the instability.

Equation (4) was derived assuming that only seven Stokes waves were present. For analytical purposes Pender and Hesselink assumed 13 waves in their analysis (12 waves uniformly spaced around the cone plus one on axis). In their numerical analysis they show that for uniform seeding of all 13 waves only ordinary conical emission results. If, on the other hand, one of the waves on the cone is seeded with a

higher intensity then the others, this wave and the other five waves making up the corresponding hexagonal intensity distribution see higher gain than the remaining six around the cone. In fact, the six waves that do not see gain actually experience loss, implying that, in this case, energy is redistributed around the cone favoring the hexagonal pattern formation. Equation (4) is in the same form as that of Pender and Hesselink, and, hence, their results are expected to apply here. Thus, it is plausible to expect a transverse modulational instability to occur in the presence of stimulated Raman scattering as was observed in the experiments discussed above.

Conclusions

Transverse modulational instabilities have been observed in an OMEGA beam in two separate experiments. In one experiment a collimated beam with 351-nm wavelength propagated through air, and the instability was observed in the presence of stimulated rotational Raman scattering. In the second experiment, the instability was observed when a 1-kJ laser pulse with 1054-nm wavelength was focused into a spatial filter having a 50-μm residual pressure. In both experiments, the transverse modulational instability took the form of a hexagonal intensity distribution in the far field of the interaction region.

A qualitative analysis of the instability can be performed in the plane-wave approximation. The instability is due to a phase-matched, four-wave-mixing interaction involving the Raman Stokes and anti-Stokes fields in the medium. The data and analysis agree well with similar work in the field. A complete analysis of the beam intensity modulation on a high-energy laser should include the effects of this transverse modulational instability.

ACKNOWLEDGMENT

The author thanks J. Kelly, K. Thorp, and M. Tedrow for experimental results that lead to Fig. 59.14 and to R. Bahr for his work on the SRRS experiment. This work was supported by the U.S. Department of Energy Office of Inertial Confinement Fusion under Cooperative Agreement No. DE-FC03-92SF19460, the University of Rochester, and the New York State Energy Research and Development Authority. The support of DOE does not constitute an endorsement by DOE of the views expressed in this article.

REFERENCES

1. M. A. Henesian, C. D. Swift, and J. R. Murray, Opt. Lett. **10**, 565 (1985).
2. M. D. Skeldon and R. E. Bahr, Opt. Lett. **16**, 366 (1991).
3. Laboratory for Laser Energetics LLE Review **52**, NTIS document No. DOE/DP/40200-229, 1992 (unpublished), p. 211.
4. N. Bloembergen, *Nonlinear Optics* (The Benjamin/Cummings Publishing Co., Inc., MA, 1982).
5. N. Tan-No, T. Hoshimiya, and H. Inaba, IEEE J. Quantum Electron. **16**, 147 (1980).
6. G. Grynberg, Opt. Commun. **66**, 321 (1988).
7. G. Grynberg *et al.*, Opt. Commun. **67**, 363 (1988).
8. A. L. Gaeta, M. D. Skeldon, R. W. Boyd, and P. Narum, J. Opt. Soc. Am. B **6**, 1709 (1989).
9. J. Pender and L. Hesselink, J. Opt. Soc. Am. B **7**, 1361 (1990).
10. R. Chang *et al.*, Opt. Commun. **88**, 167 (1992).
11. J. B. Geddes, J. V. Moloney, and R. Indik, Opt. Commun. **90**, 117 (1992).
12. J. Y. Courtois and G. Grynberg, Opt. Commun. **87**, 186 (1992).
13. M. Tamburrini *et al.*, Opt. Lett. **18**, 855 (1993).